ORNL/TM-2023/3048

FY23 Progress Report on Viscosity and Thermal Conductivity Measurements of Molten Salts

Anthony Birri
Nicholas Termini
Kevin Garland
Shay Chapel
Hunter Andrews
Paul Rose Jr.
N. Dianne Bull Ezell

OAK RIDGE
National Laboratory

ORNL IS MANAGED BY UT-BATTELLE LLC FOR THE US DEPARTMENT OF ENERGY

DOCUMENT AVAILABILITY

Reports produced after January 1, 1996, are generally available free via OSTI.GOV.

Website: www.osti.gov/

Reports produced before January 1, 1996, may be purchased by members of the public from the following source:

National Technical Information Service
5285 Port Royal Road
Springfield, VA 22161
Telephone: 703-605-6000 (1-800-553-6847)
TDD: 703-487-4639
Fax: 703-605-6900
E-mail: info@ntis.gov
Website: http://classic.ntis.gov/

Reports are available to DOE employees, DOE contractors, Energy Technology Data Exchange representatives, and International Nuclear Information System representatives from the following source:

Office of Scientific and Technical Information
PO Box 62
Oak Ridge, TN 37831
Telephone: 865-576-8401
Fax: 865-576-5728
E-mail: report@osti.gov
Website: https://www.osti.gov/

This report was prepared as an account of work sponsored by an agency of the United States Government. Neither the United States Government nor any agency thereof, nor any of their employees, makes any warranty, express or implied, or assumes any legal liability or responsibility for the accuracy, completeness, or usefulness of any information, apparatus, product, or process disclosed, or represents that its use would not infringe privately owned rights. Reference herein to any specific commercial product, process, or service by trade name, trademark, manufacturer, or otherwise, does not necessarily constitute or imply its endorsement, recommendation, or favoring by the United States Government or any agency thereof. The views and opinions of authors expressed herein do not necessarily state or reflect those of the United States Government or any agency thereof.

ORNL/TM-2023/3048

Nuclear Energy and Fuel Cycle Division

FY23 PROGRESS REPORT ON VISCOSITY AND THERMAL CONDUCTIVITY MEASUREMENTS OF MOLTEN SALTS

Anthony Birri
Nicholas Termini
Kevin Garland
Shay Chapel
Hunter Andrews
Paul Rose Jr.
N. Dianne Bull Ezell

Milestone M3AT-23OR0804071
August 2023

Prepared by
OAK RIDGE NATIONAL LABORATORY
Oak Ridge, TN 37831
managed by
UT-Battelle LLC
for the
US DEPARTMENT OF ENERGY
under contract DE-AC05-00OR22725

CONTENTS

LIST OF FIGURES

ACKNOWLEDGMENTS

This work is funded by the US Department of Energy’s Office of Nuclear Energy, Molten Salt Reactor (MSR) Campaign under the Advanced Reactor Technology (ART) program. The authors would like to thank Joanna Mcfarlane, and Kevin Robb for their insights and expertise regarding molten salt chemistry, handling, and experimental considerations.

ABBREVIATIONS

DOE-NE	US Department of Energys Office of Nuclear Energy
MSR	molten salt reactor
MSTDB-TP	Molten Salt Thermal Properties Database–Thermophysical
NEAMS	Nuclear Energy Advanced Modeling and Simulation
NIST	National Institute of Standards and Technology
NRC	Nuclear Regulatory Commission
ORNL	Oak Ridge National Laboratory

SUMMARY

As presented in this report, thermal conductivity and viscosity measurements were performed on key chloride pseudo-binary molten salt systems of relevance to molten salt reactor developers. Thermal conductivity measurements were conducted with a variable gap technique, in which a known heat flux is driven across a molten salt specimen and the temperature difference is measured, allowing calculation of the thermal conductivity. This is achieved by establishing a small gap between the bottom of a cylindrical inner containment, which houses electrical heating elements, and an outer containment, which houses cooling channels; the gap size can be varied by compression of a formed bellows. A new calibration scheme was developed herein, involving a correction factor to the heat flux based on He measurements at various temperatures. Furthermore, the data processing methodology was improved to minimize the impact of radiative heat transfer in the calculation of salt specimen thermal conductivity from the temperature difference measurements. Viscosity measurements were conducted with a rolling ball viscometer, in which a ball rolls some known distance in an angled tubular crucible, and the terminal velocity can be used to calculate the viscosity of the salt. The measurement can be performed in a quartz crucible, with which a standard camera can be used to track the ball, or in a metal crucible, with which x-ray radiography is required to track the ball. A new custom x-ray system was made and dedicated to the rolling ball viscometer to enable high throughput automated measurements with salts which require containment with metal. Both systems have been integrated with a ventilation stack which allows for off-gassing of radioactive material, enabling future measurements with U-bearing salts.

The thermal conductivity measurements performed herein were with NaCl-KCl (44 mol% NaCl). This salt system was measured in the previous fiscal year, however the thermal conductivity values obtained were comparatively low, and so the system was remeasured with the aforementioned calibration scheme and improved post-processing techniques. The newly obtained thermal conductivity values for NaCl-KCl (44 mol% NaCl) indicate good agreement with kinetic theory and ab-initio models (within 5–10 %). The viscosity measurements performed herein were with three different compositions of NaCl-KCl: 75, 50, and 25 mol% NaCl; a new calibration scheme was applied to account for variable flow effects in the laminar regime. The results show reasonable agreement with literature (5–20 %, depending on the temperature, composition, and study); however, literature values are likely higher than true values based on pure end-member measurements performed in the comparative studies. The measurements conducted herein do show a trend such that viscosity increases with increasing NaCl concentration, which agrees well with one of two comparative studies. In general, the measurements conducted herein gives confidence in the capability to use these systems to accurately measure thermal conductivity and viscosity of actinide-bearing salts within the next fiscal year.

1. INTRODUCTION

Several private and public domestic entities are in the process of designing, developing, licensing, and demonstrating molten salt reactor (MSR) designs. The intent of these projects is ultimately to deploy MSR designs so that they can contribute to the energy grid [9, 22, 27, 29, 45] or serve as experimental test reactors [47]. These designs are considering a wide range of molten halide salt mixtures: those of a variety of mixture orders and actinide compounds in the fuel mixtures, some that are both chloride and fluoride based, and some that consider beryllium. The cumulative interest in different salt mixtures from the domestic industry has resulted in a large matrix of potential salt mixtures for MSR applications; this matrix was first been defined by McMurray in a roadmap for molten salt thermal property measurements [34]. Consequently, a complete and accurate characterization of the thermophysical properties of this matrix is desired. These thermophysical properties primarily include density, viscosity, thermal conductivity, and heat capacity. In addition, knowledge of the surface tension and optical properties may be desired. Without accurate thermophysical characterization of a particular salt mixture in question for a particular MSR design, thermal hydraulics or mass transfer analysis cannot be performed, which would be necessary to understand aspects of core performance such as the temperature distribution in steady-state or transient conditions. Moreover, the U.S. Nuclear Regulatory Commission (NRC) will likely require a well-described thermal hydraulic design as well as analysis of accident scenarios (such as behaviour during power–cooling mismatch events) before licensing a particular MSR design [5]. Furthermore, a complete thermophysical description of many of the salt mixtures in the matrix of MSR relevant mixtures will be needed to allow MSR developers to more easily optimize their selection of a particular mixture and composition that fits their criteria.

Unfortunately, there are several thermophysical property gaps within the matrix of molten salt mixtures that are of concern in the development of MSR designs. These gaps are presented in a recent report on the thermophysical arm of the Molten Salt Thermal Properties Database (MSTDB-TP) [46], which is managed at Oak Ridge National Laboratory (ORNL), with funding from the Nuclear Energy Advanced Modeling and Simulation (NEAMS) program under the US Department of Energy's Office of Nuclear Energy (DOE-NE). For example, though perhaps density is reasonably well understood for many key mixtures, several key pseudo-binary mixtures lack characterization for viscosity, thermal conductivity, and heat capacity. Furthermore, significant discrepancies tend to be present in independent measurements of these properties for the same mixtures: for example, independent studies of eutectic LiF-NaF-KF thermal conductivity have yielded values as low as 0.5 W/mK to as high as 4 W/mK for the same temperature [2].

Several gaps in thermophysical property data for key mixtures may be expected, and high uncertainties are common for the data that do exist; in general, the salt mixtures that are of interest for MSR developers can be highly corrosive, hygroscopic, volatile, and difficult to purely synthesize. Furthermore, developing and maintaining systems that can handle the use of potentially toxic and radioactive salts at extreme temperatures require significant capital investment, personnel costs, and expertise in manufacturing and operating such systems. Therefore, experimental efforts across the national laboratory complex and university research laboratories represent only one current strategy to fill gaps in molten salt thermophysical data. First-principles modeling techniques such as ab initio [40, 26, 33, 41, 32, 31, 30, 20, 12, 11, 10, 39] and semi-empirical approaches such as modified quasi-chemical [38, 17] and Redlich–Kister [1, 6] methods have been developed and demonstrated to fill some of the gaps as well. If an MSR developer were to utilize such models to hone in on a particular salt mixture and composition of interest, further experimental validation of the models for that particular composition would likely be required for NRC licensing.

Given the apparent need for high-accuracy measurements of key pseudo-binary and perhaps certain higher-order salt mixtures, Oak Ridge National Laboratory (ORNL) has focused on developing and demonstrating systems capable of measuring each of the thermophysical properties, focusing particularly on thermal conductivity and viscosity, due to the generally poor or non-existent characterization in the literature for these two properties. ORNL recognizes that characterization of heat capacity is generally lacking for many key mixtures as well, but other DOE-NE funded laboratory and university partners are focusing more heavily on measurements of that property specifically [15, 14, 23, 28, 42, 50]. The molten salt mixtures measured herein—and which have been measured in previous reports on this work [8, 16]—are all alkali halide mixtures, which represent either coolant salts or subsystems to higher-order actinide-bearing salts that may be considered as MSR fuel. However, the measurement systems developed and reported on herein have been designed to enable direct measurements of actinide-bearing mixtures, which will be crucial for providing accurate and validated thermophysical property data to MSR thermal models.

2. VISCOSITY MEASUREMENT SYSTEM

2.1 METHODOLOGY

2.1.1 Principles of Operation

A rolling-ball viscometer was chosen by ORNL as the technique to measure molten salt viscosity. The system involves rolling a ball through a tubular crucible filled with molten salt and measuring the time, t, that the ball takes to roll some length, L, through the crucible, which is tilted at some angle, θ. The working equations to solve for the viscosity, μ, of the salt involve force balance of the three forces that act on the ball along the crucible's axial direction: (1) the opposing viscous force, (2) the opposing buoyancy force, and (3) the gravitational driving force. It can be shown [7] that, by solving for μ in these equations, one arrives at

$$\mu = \frac{K(\rho_b - \rho_f)tsin(\theta)}{L}, \tag{1}$$

where K is a geometric correction factor, ρ_b is the density of the ball, and ρ_f is the density of the fluid (molten salt). Here, K depends on the Reynolds number associated with the flow, Re, and the ratio of the ball diameter to the inner diameter of the crucible, d/D. It has also been shown [7] that, for some Re value, a polynomial-type equation works well to describe this relationship:

$$K\Big(Re, \frac{d}{D}\Big) = a(Re) + b(Re)\Big(\frac{d}{D}\Big) + c(Re)\Big(\frac{d}{D}\Big)^2, \tag{2}$$

where a, b, and c are constants that can be determined through a least-squares fit to data at a particular Re.

In this work, the crucible and ball were not fabricated with the same material; the crucible was fused quartz, whereas the balls were stainless steel 316 alloy. Therefore, these components had different coefficients of thermal expansion, meaning that d/D was temperature dependent. Therefore, this work required the measurement of many K values—over a wide range of Re and d/D values—using National Institute of Standards and Technology (NIST) oils with well-known viscosities to adequately characterize the variable space associated with Eq. (2). Details on handling the temperature dependence of d/D to accurately determine d/D for any temperature can be found in Birri et al. [7]. Thermal expansion data to solve for d/D at varying temperatures were acquired from studies by Kim [25] and Oishi [37].

Given that the appropriate K value is assigned to a measurement of μ in the salt at a given temperature T, and many measurements are collected over a range of T values, an Arrhenius-type equation is assumed to describe the functional relationship between μ and T:

$$\mu(T) = Ae^{B/RT}, \tag{3}$$

where A and B are constants determined based on a least-squares fit to measured μ values at different T values, and R is the universal gas constant.

2.1.2 System Overview

As opposed to designs in previous reports [8, 16], a simplified, two-stage crucible design was designed and fabricated in this work, as shown in Figure 1. The crucible consists of a loading section (i.e., the first stage) and a measurement section (i.e., the second stage). The loading section is intended to hold the ball after loading until the ball has reached thermal equilibrium with the system; this is achieved when the crucible is rotated such that the ledge between the measurement section and the loading section is on the underside of the crucible, preventing the ball from rolling into the measurement section. The measurement section contains two etch marks (labeled as I and II in Figure 1) that define L; these marks are used to measure t as the ball rolls through the measurement section. The ball can enter the measurement section when the crucible is rotated such that the ledge between the measurement section and the loading section is on the overside of the crucible, and the underside of the crucible has a flush transition between both stages. Previously fabricated designs involved a third stage, which was a second holding section; the intent was to be able to tilt the crucible back and forth, conducting multiple measurements with the same ball. However, gas pocket formation was an issue with this design implementation [8]. The simplified design considered herein remains in a static orientation, and new balls are introduced to the crucible for each measurement.

During testing, the crucible is inserted into a tube furnace as shown later in Section 4 in Figure 11, which is oriented on a manipulable test stand. The test stand allows the furnace to be tilted to a desired angle, which is measured with a digital angle gauge. The furnace has a small viewing window in the insulation to allow for visual tracking of the ball if a glass crucible is used or to minimize x-ray attenuation if an x-ray generator and x-ray detector plate system are used in conjunction with a metal crucible. The crucible is attached to a rotational stage, which enables the rotation to drop the ball from the loading section to the measurement section. The rotational stage is mounted on a linear motion stage to ensure proper orientation within the tube furnace. An argon backfill system is connected to the crucible to ensure inert gas maintenance within the crucible volume at all times. The system comes equipped with a vacuum pump to enable backfilling of the entire control volume as well as vacuum heating of the salt for dehydration, if desired. The system also has an argon feed line, a large tank to minimize pressure increases from heating the salt, and a small load-lock chamber to allow new balls to enter the system without contaminating the inert environment. Temperatures are measured with type-N thermocouples oriented adjacent to the crucible. Additional details about this system, including exact components and specifications, can be found in Birri et al. [7].

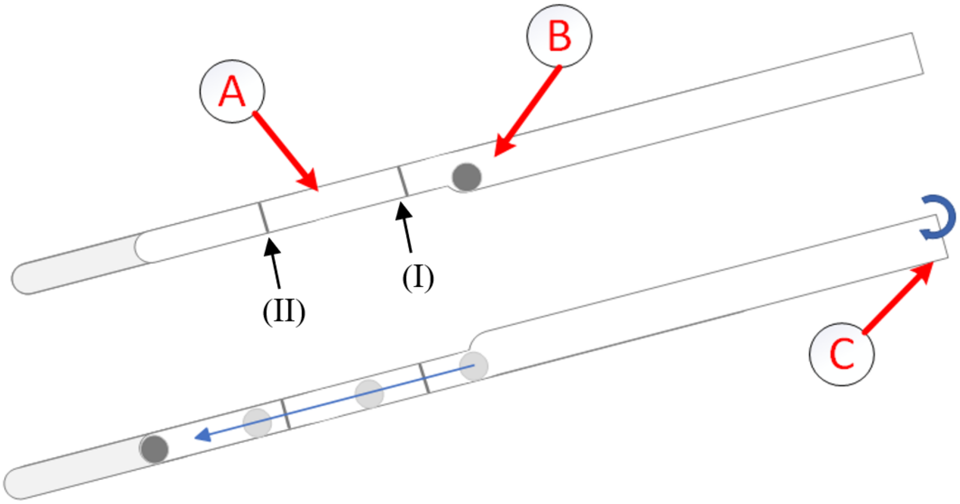

Figure 1. Two separate crucibles demonstrating the change in orientation in the experimental apparatus. The top represents the initial position where the ball is held in the holding section. The bottom represents a 180° turn to a final position allowing the ball to descend. A, measurement section; B, holding section; and C, the entrance to the crucible attached to the rotational stage and argon inert environment.

2.2 SYSTEM CAPABILITY EXPANSION

The rolling ball viscometer developed herein was improved in two primary ways during FY23: (1) implementation of a new, dedicated x-ray system, as opposed to a portable system, and (2) integration to a ventilation stack that captures internal off-gasses, enabling measurements of uranium-bearing salts. Both of these system improvements are intended to enable handling of compounds such as UCl_3, UCl_4, UF_3, UF_4, and fluoride alkali halides. The dedicated x-ray system is crucial for such compounds because they require containment in alloys such as stainless-steel 316, or perhaps more corrosion-resistant alloys such as Hastelloy or nickel-dominant alloys; tracking balls in these alloys requires x-ray imaging techniques. Furthermore, these improvements advance the system toward more high-throughput measurements. Because of the 100% x-ray imaging system dedication for anytime use, Python scripts can be used to communicate simultaneously with the imaging system and automated rotational stage for semi-autonomous experimentation and data acquisition.

The x-ray generating device used previously is described in detail in previous works [43]. The setup consisted of a mobile XRS4 from Golden Engineering producing a 370 kVp bremsstrahlung beam. Images were generated using a NOVO 22WN digital radiography panel, and a fast plastic scintillator (EJ-200 from Eljen Technologies) was placed next to the XRS4 and connected to a CAEN DT5730 digitizer. The new x-ray imaging system uses a XRS4T from Golden Engineering with the same kilovoltage peak as the previously implemented generating device, which is now dedicated to the viscometer 100% of the time; it is automatically triggerable, whereas the XRS4 was self-triggered. The trigger signal can be sent from a Python script over USB/RS232 converter to the device. X-ray images are generated in the new system using a Varex XRD 3025N-G22-N; the device can be operated using commercial software, and APIs are available that can be called in Python for both controls and image acquisition. Also, this panel has a 5 fps frame rate which will enable video generation, as opposed to a series of static images, which were generated previously with the NOVO 22WN and required more significant post-processing to determine terminal velocities. In Section 4, the new x-ray system is shown in Figure 11, along with the entire viscosity and thermal conductivity system setups; the detector plate is not visible, as it is behind the furnace in this image.

2.3 IMPROVEMENTS TO METHODOLOGY

Previously [8, 7], it was assumed that $K\left(Re, \frac{d}{D}\right)$ consisted of two primary regimes in the Re space: (1) a Stoke's flow regime for $Re << 1$ and (2) a laminar regime for $Re > 10$, with a transition between both regimes. The laminar regime was assumed to be a plateau, such that $\partial K/\partial Re \approx 0$. Herein, calibration measurements were taken at higher Re numbers and lower d/D values than considered previously, which resulted in the discovery that $\partial K/\partial Re < 0$ for relatively low values of d/D in the laminar regime, and this is more consequential for high values of Re. Regardless, in light of this discovery, it was crucial to modify the manner in which K values were assigned to salt viscosity measurements for the sake of improving accuracy of the overall measurement scheme. Note that all salts considered herein and in previous works involved measurements in the laminar regime, so the focus on tuning the determination of K strictly involves the assumption that the salt viscosity is low enough to result in measurements in this regime.

The calibration involves measurements with NIST standard oils with well-known viscosities for a range of d/D values, such that a total of I values are considered with index i. Therefore, it is assumed that for some d/D at which a given crucible is calibrated ($(d/D)_i$), $K(d/D = (d/D)_i, Re)$ follows a linear relationship:

$$K(d/D = (d/D)_i, Re) = a_i + b_i * Re, \tag{4}$$

where a_i and b_i are constants determined based on a least-squares fit to raw data acquired for $K(d/D = (d/D)_i, Re)$. A total of I calibration curves, of the form of Eq. (4), exist in the calibration data: here, $I = 4$. Assuming a salt measurement takes place at some calculated $(d/D)_m$, then it is assumed that there is some respective linear relationship that describes $K(d/D = (d/D)_m, Re)$:

$$K(d/D = (d/D)_m, Re) = a_m + b_m * Re, \tag{5}$$

where a_m and b_m are assumed to be weighted averages of the constants in the calibration curves associated with the $(d/D)_i$, which is immediately below that associated with $(d/D)_m$—and the calibration curves associated with the $(d/D)_{i+1}$, which is immediately above that associated with $(d/D)_m$. These weighted averages thus take the form

$$a_m = \frac{|(d/D)_m - (d/D)_i|}{|(d/D)_{i+1} - (d/D)_i|} a_i + \frac{|(d/D)_m - (d/D)_{i+1}|}{|(d/D)_{i+1} - (d/D)_i|} a_{i+1} \quad if\ (d/D)_i < (d/D)_m < (d/D)_{i+1}, \tag{6}$$

$$b_m = \frac{|(d/D)_m - (d/D)_i|}{|(d/D)_{i+1} - (d/D)_i|} b_i + \frac{|(d/D)_m - (d/D)_{i+1}|}{|(d/D)_{i+1} - (d/D)_i|} b_{i+1} \quad if\ (d/D)_i < (d/D)_m < (d/D)_{i+1}. \tag{7}$$

After determination of a_m and b_m associated with $K(d/D = (d/D)_m, Re)$, an iterative process is applied to solve for Re because Re depends on μ. Thus, some guess values for μ are initially supplied, Re is calculated from this guess, and then $K(d/D = (d/D)_m, Re)$ is used to determine an updated value for μ. This process is repeated until some residual criterion is met.

An example of the calibration curves used—that is, $K(d/D = (d/D)_i, Re)$—for one particular crucible is shown in Figure 2. The four $(d/D)_i$ values are shown in the legend. The a_i and b_i values associated with these curves are used to determine a_m and b_m for any given salt measurement, based on Eqs. (6) and (7).

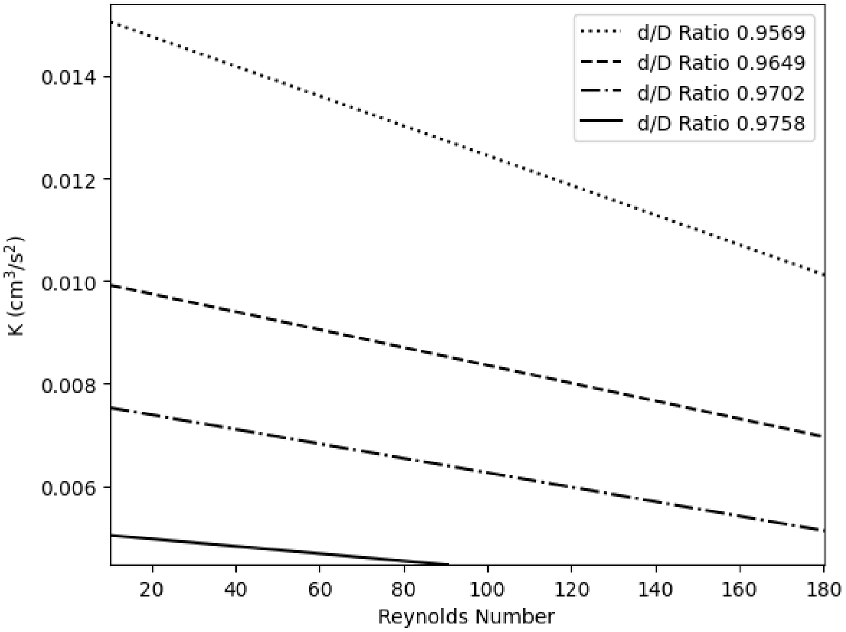

Figure 2. $K(d/D = (d/D)_i, Re)$ **for one particular glass crucible, determined based on non-linear least squares fitting to NIST oil measurements.**

It should also be noted that, the formalism was developed in this FY to apply propagation of uncertainty to experimentally acquired viscosity data for molten salts. This propagation is based on Gaussian error formalism, where the uncertainties associated with d, D, K, ρ_b, ρ_f, t, θ, L, and T are all input to a set of dependent equations to solve for the uncertainty in μ. This formalism is fully detailed in Birri et al. [7]. Experimental uncertainties reported in the next section were determined based on application of this same formalism.

2.4 EXPERIMENTAL MEASUREMENTS

A compositional study on the viscosity of NaCl-KCl was conducted in this work for mixtures of 0.75, 0.50, and 0.25 mol% NaCl. Each crucible used for this measurement was calibrated separately such that a unique set of calibration curves was applied to each crucible to convert terminal velocity to viscosity. All salt samples were vacuum dried at 350°C for ~4 h prior to heating and melting at the maximum temperature set point associated with a given mixture. The samples were then allowed to homogenize at the maximum temperature set point for ~16 h before viscosity measurements were conducted. Each salt mixture was measured at four temperature set points in triplicates, such that the lowest temperature set point was ~25–45°C above the mixture's respective melting point. Mixture melting points were determined based on phase diagrams generated in FactSage (version 8.2) using the thermochemical arm of MSTDB (MSTDB-TC) [4]; the NaCl-KCl evaluation has been validated against the works of Yin [49]. Densities of the salt were calculated based on a Redlich–Kister model which was fit to experimental data from Van Artsdalen [48].

A plot of the experimental data collected herein is shown in Figure 3, along with similar mixtures measured by Murgulescu [35] and Katyshev [24]; identical colors are used to compare mixtures that are identical or most similar across these studies. As discussed in previous works by the authors with NaCl-KCl, [7] it is generally expected that Murgulescu and Katyshev may have erroneously high measurements of viscosity of NaCl-KCl, because both authors report high-endmember viscosity data relative to reference values. However, the overall trend in viscosity as a function of composition is similar between Murgulescu and this work, such that the viscosity increases by ~0.2–0.3 cP as NaCl concentration is increased from ~25 to 75 mol %. Contrarily, Katyshev did not observe a trend as obvious as that regarding viscosity as a function of composition.

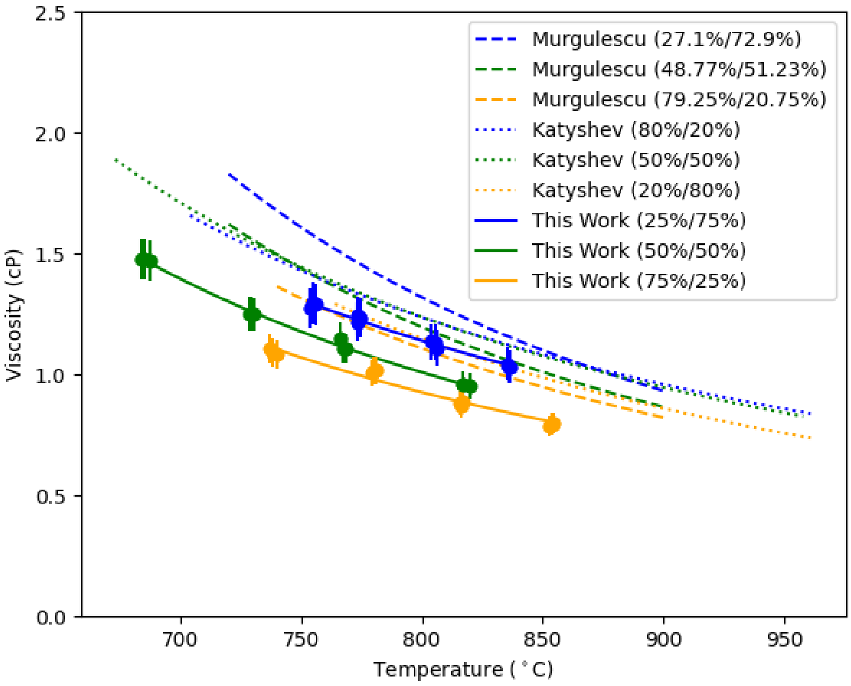

Figure 3. Measured viscosity of NaCl-KCl as a function of temperature and composition. Data comes from this work and values from the literature.

These measurements performed with NaCl-KCl are part of a larger effort to characterize the pseudo-ternary system NaCl-KCl-LiCl and the pseudo-ternary subsystems. Such an effort demonstrates the high-throughput measurement capabilities with the rolling ball viscometer, thus enabling full compositional studies of higher-order systems. Measurements are being validated against those in the literature and ab initio simulations, following the general framework described in Nguyen et al. [36]. Laser-induced breakdown spectroscopy is also being performed for trace metal and moisture content

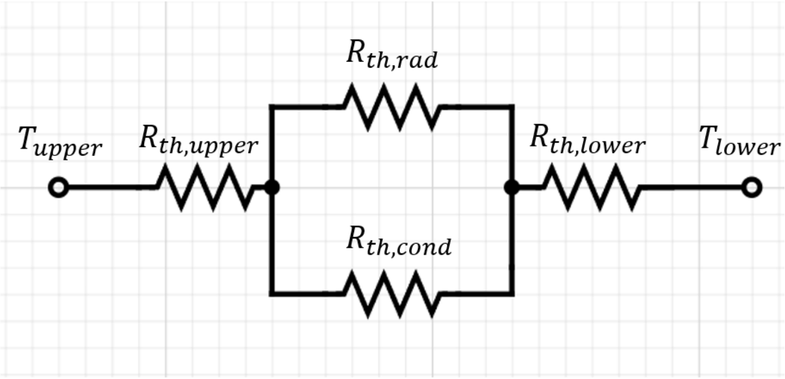

Figure 4. Circuit diagram that describes the electrical analog to the thermal resistances associated with the variable gap technique.

analysis, following processes described in Andrews and Phongikaroon [3].

3. THERMAL CONDUCTIVITY MEASUREMENT SYSTEM

3.1 METHODOLOGY

3.1.1 Principles of Operation

Thermal conductivity measurements of molten salts at ORNL are performed using the variable gap technique. This technique was developed in 1973 by Cooke [13] and adapted by Gallagher [18, 19]; the system developed by Gallagher is considered herein. The variable gap technique is a steady-state technique involving careful measurement of temperature difference across a gap with a fluid specimen with unknown thermal conductivity while driving a known heat flux across. The main advantage of the variable gap technique over other steady-state measurement techniques is that measurements at different salt thicknesses (gaps) allow the conductivity to be dependent only on the salt properties, and not the other materials in the system (fixed resistance).

Using the electrical circuit analog, the system can be described using Figure 4. T_{upper} and T_{lower} represent the temperatures, which are measured by the probes located on the upper and the lower ends of the specimen, respectively. $R_{th,upper}$ and $R_{th,lower}$ are the thermal resistances associated with the material between the probes and the specimen on the upper and lower ends of the specimen, respectively. The specimen itself has three heat transfer mechanisms; therefore, it should have three resistances in parallel (radiation $R_{th,rad}$, conduction $R_{th,cond}$, convection). However, convection is considered negligible for the small gap sizes measured, proven based on an assessment of the Rayleigh number in Gallagher et al. [18].

The total fixed resistance in the system is defined as

$$R_{th,fixed} = R_{th,upper} + R_{th,lower}, \tag{8}$$

and the total variable resistance in the system is defined as

$$R_{th,var} = \frac{1}{\kappa_{cond} + \kappa_{rad}}, \tag{9}$$

where κ_{cond} is the thermal conductivity of the salt, and κ_{rad} is the effective radiative component. Using Fourier's law, the conductivity as a function of specimen thickness or gap size (x) can be defined:

$$\frac{\Delta T_{spec}(x)}{q''} = R_{th,fixed} + \frac{1}{\kappa_{cond} + \kappa_{rad}} x, \tag{10}$$

where q'' is the heat flux applied by some heat source on the upper end of the specimen, and $\Delta T_{spec}(x)$ is the difference between T_{upper} and T_{lower}. By measuring the ΔT_{spec} at multiple x values, a linear function can be fit, where $\frac{1}{\kappa_{cond}+\kappa_{rad}}$ is the slope of the line. From this slope value, thermal conductivity κ_{cond} can be determined by calculating the radiative component κ_{rad}, which depends on the optical properties of the salt-wetted faces above and below the specimen, and of the salt specimen itself.

The main challenges for accurately measuring thermal conductivity in this system are accounting for system effects (heat losses/gains) on q'' and the correction of κ_{rad}, which is discussed in more detail in section 3.2.

3.1.2 System Overview

An overall view of the thermal conductivity system is shown in Figure 5. The system comprises an external and internal containment. The structure is compact enough to fit within a glove box for specimen loading. The containment can then be resealed inside the glove box after loading such that the salt is never exposed to an open environment and is always in an inert one. The system is then placed inside a tube furnace, where it can be heated up to temperatures of 900°C. Air is flowed through the bottom of the external containment through evenly spaced channels, while two heating elements, a main heater and a guard heater, are placed inside the bottom of the internal containment above the sample shown in Figures 6 and 7. The two heating elements drive a ΔT across the sample. The internal containment can move vertically via a welded bellows feedthrough, which allows the heating elements to move farther down into the outer containment. This, in turn, reduces the amount of salt sampled and changes the gap thickness (x). This gap thickness is measured by a digital variance indicator following the internal containment. Two complete containment structures have been constructed from Hastelloy C-276 and SS-316; both are available for salt measurements.

3.2 IMPROVEMENTS TO METHODOLOGY

Over this FY, significant work was devoted to reducing the uncertainty and increasing the consistency in measurements. Two parameters were identified that influenced the measurements the most significantly: heat flux (q'') and radiative heat transfer (k_{rad}).

In previous measurements, heat flux into the sample was solely determined to be from the "main" heater, with the assumption that heat shunting in the system was low if the system was properly insulated and ΔT between the main heater and the top of the guard heater was close to 0. However, it was determined

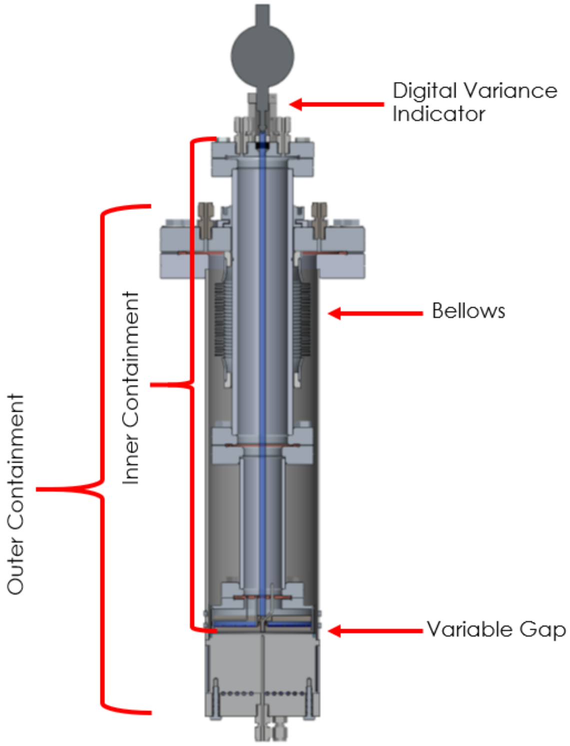

Figure 5. Overall cross-sectional view of the variable gap system, which comprises the inner and outer containments.

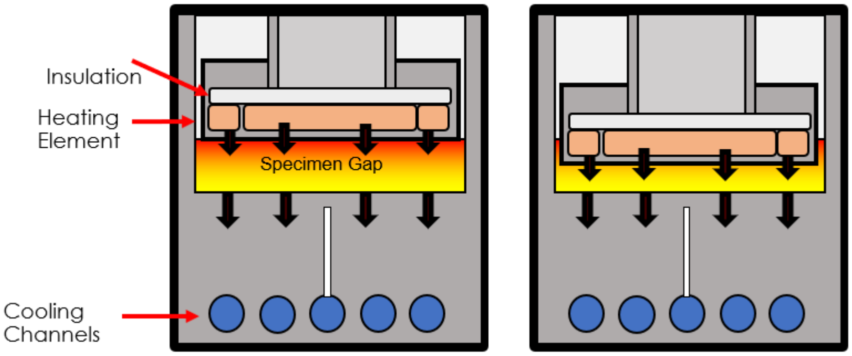

Figure 6. Specimen region of the variable gap system. Black arrows indicate ideal heat flux vectors.)

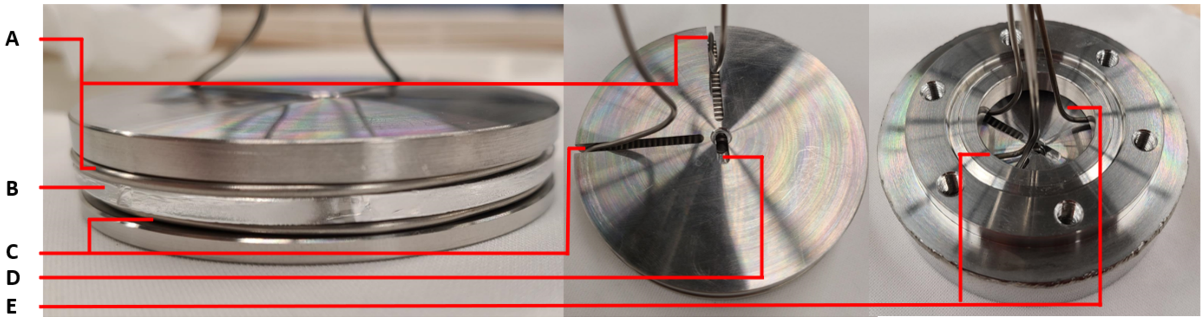

Figure 7. As-built heater assembly: (a) axial guard heater, (b) quartz insulator, (c) main heater, (d) center thermocouple slot, and (e) side thermocouples placed in welded heater assembly cup.

through repeated measurements with various media that this assumption was not accurate, and it was too difficult to ensure perfect insulation to prevent excessive heat shunting and to maintain the ΔT assumption over repeated measurements. Even if the difference between main heater and guard heater temperatures were low—especially if there were a large discrepancy in power supplied to each heater—the system could not accurately predict thermal conductivity. Therefore, a more rigorous characterization of heat flux was performed using various helium calibrations at different temperatures and systems setups to establish a correction factor (C_S) to account for heat shunting based on temperature profiles within the system:

$$\frac{\Delta T_{spec}(x)}{(C_S)(q'')} = R_{th,fixed} + \frac{1}{\kappa_{cond} + \kappa_{rad}} x, \tag{11}$$

This power correction is assumed to correct for the following:

- Radial losses/gains
- Combined power contribution to the salt from both main and guard heater
- Differences in cooling power from measurement to measurement

To ensure that the heat loss characteristics are similar from a helium calibration to a salt measurement, it was assumed that for a given measurement, if the magnitude of ΔT_{spec} is the same, a power correction for one measurement can be applied to another measurement. Figure 8 shows the power correction trends as a function of ΔT_{spec}.

The second major source of uncertainty is radiative heat transfer. With the addition of helium as a calibrator for the system, the differences in how media interact with radiation must be accounted for. Helium is considered transparent (i.e., negligible interaction with radiation), whereas salt is considered optically thin but participating. Both media have significant but different effective radiative heat transfer components. Therefore, when determining the power correction factor during calibration, the inherent transparent radiative heat transfer must be accounted for before applying this correction to the salt (which will have its own but different relationship). In previous considerations of the radiative heat transfer, both effective radiative conductivities (transparent and optically thin but participating) were presented as κ_{rad} in [18] as:

$$\kappa_{rad_{He}} = \frac{\epsilon \sigma x (T_{upper} + T_{lower})(T_{upper}^2 + T_{lower}^2)}{2 - \epsilon}, \tag{12}$$

$$\kappa_{rad_{salt}} = 4\bar{n}^2 \epsilon \sigma T_{spec}^3 x, \tag{13}$$

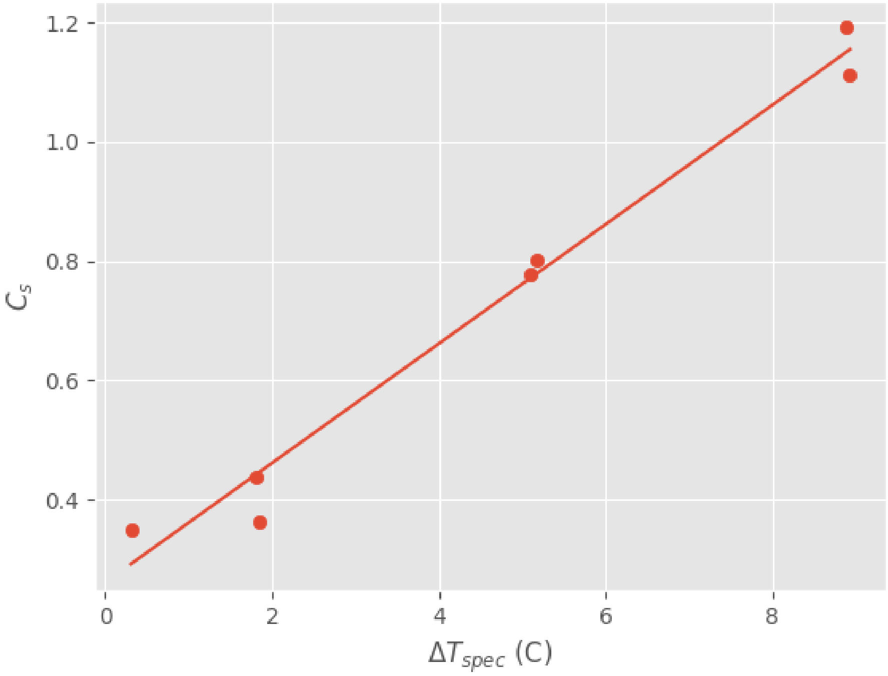

Figure 8. Changes in the power correction factor C_s due to heat shunting with respect to the difference in temperature across the specimen (T_{spec}) .

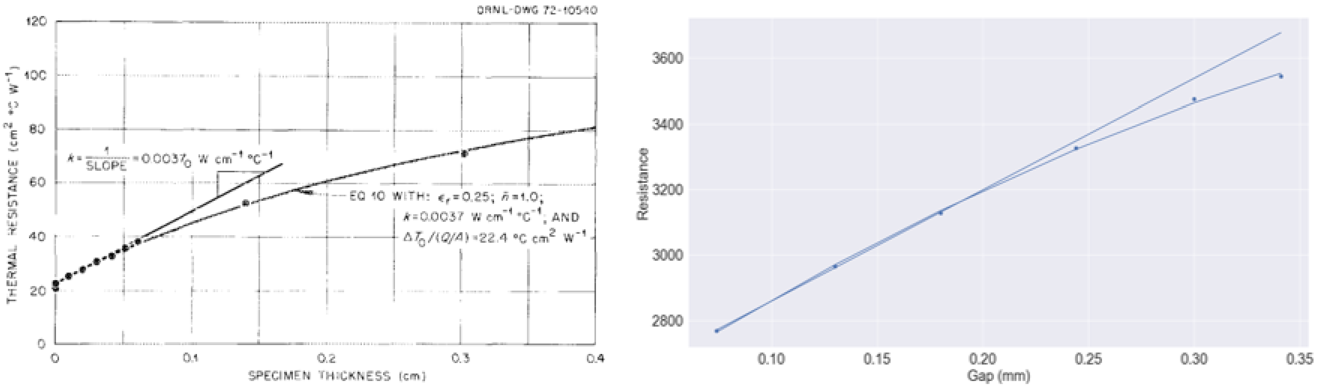

(a) (b)

Figure 9. Radiative heat effect on resistance curves during gap changes for (a) 900°C helium [13] and (b) 700°C helium (Current).

where ϵ is emissivity, T_{spec} is average specimen temperature, and $\bar{n}$ is the refractive index of the salt. However, singling out the radiative heat transfer for calculating the power correction factor or correcting the salt conductivity are very challenging due to the dependence of κ_{rad} on x. It is also very challenging to directly calculate the radiative heat transfer because the emissivity of the plates is constantly changing and difficult to determine, and optical properties of the salt ($\bar{n}$) are not well studied. Therefore, an experimental approach was taken to remove the effect of radiative heat transfer. Due to the dependence of effective radiative heat transfer on x, it can be neglected in the working equation if the slope of the resistance line is taken as close to a gap size of 0 as possible, resulting in Eq. (11) reducing to

$$\frac{1}{C_s q''} \frac{d\Delta T(x \rightarrow 0)}{dx} = \frac{1}{\kappa_{cond} + \cancelto{0}{\kappa_{rad}}} \tag{14}$$

The effects of gap size on the resistance curves due to radiative heat transfer were studied extensively by Cooke [13], and the linearizing phenomenon of the total thermal resistance as x approaches zero is seen in recent measurements taken (Figure 9); this phenomenon was similarly shown by Cooke, indicating that radiative heat transfer indeed becomes negligible for particularly small x values.

3.3 EXPERIMENTAL MEASUREMENTS

Near-minimum liquidus NaCl-KCl (44 mol% NaCl) molten salt was measured at four temperatures over the range of 680–800°C. The salt composition was loaded into the external containment, sealed, and vacuum dried at 350°C for three hours. The containment was backfilled with helium after drying to closely match the system configuration of the helium calibration measurements. For each measurement temperature, the system was given ~12 hours to reach thermal equilibrium. Temperatures were measured for each data point over five gaps ranging from 0.35 mm to 0.05 mm. The results of four temperature setpoints (680, 716, 760, and 800°C) are shown in Figure 10 comparing data from the previous FY [8], experimental literature data from Smirnov [44], kinetic theory based on a model derived by Gheribi [21], and an ab inito model [21].

The newest acquired data agree very well with kinetic theory over the temperature range measured, showing a slight negative trend with increasing temperatures.

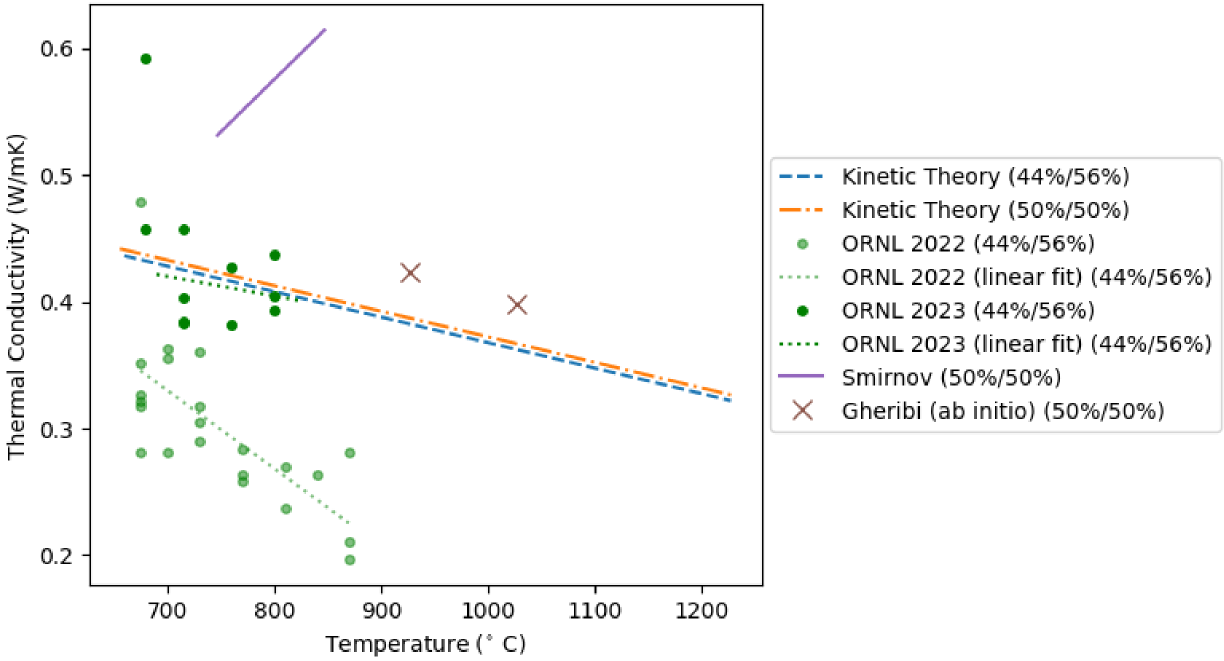

Figure 10. Comparison of new NaCl-KCl thermal conductivity measurements to previously acquired values and literature values.

Although significant variability was observed for each temperature, precision can be improved in future measurements by taking more gap measurements toward the lower gap sizes to more accurately capture the non-radiative linear trend. To further validate this new methodology, and prior to moving toward application to actinide-bearing salts, pure LiCl will be measured in the same device because LiCl is well characterized in the literature. This method will also be repeated for FLiNaK in our separate fluoride containment vessel (Hastelloy) to ensure that this methodology is validated for both containment types.

4. PREPARATION FOR URANIUM-BEARING SALT MEASUREMENTS

An image of the the variable gap thermal conductivity system and the rolling ball viscometer is shown in Figure 11. The control volumes of both of these mixtures are now connected to a ventilation stack that is designed to handle off-gassing of uranium-bearing salts. Before and after measurements with either system, the respective control volume can be completely evacuated into the stack. During measurements, an in-line pressure relief valve will be connected to the stack, such that if either system pressure exceeds its respective pressure limit, then the pressurized gas can vent into the stack as well. Such a ventilation system will be crucial because uranium-bearing salt mixtures are targeted for future experiments with both systems, now that the ability to measure thermal conductivity and viscosity of alkali halides has been established. Target compounds include UCl_3, UCl_4, UF3, and UF4, mixed with alkali halides. Regarding the chlorides, extra caution must be taken with UX_4 (where X is either fluorine or chlorine) because the U/UX_4 redox potential is relatively low [51], meaning corrosion of most metal alloys becomes thermodynamically favorable; it may be necessary to handle UX_4 (unless mixed with UX_3) in glass liners within metal alloys.

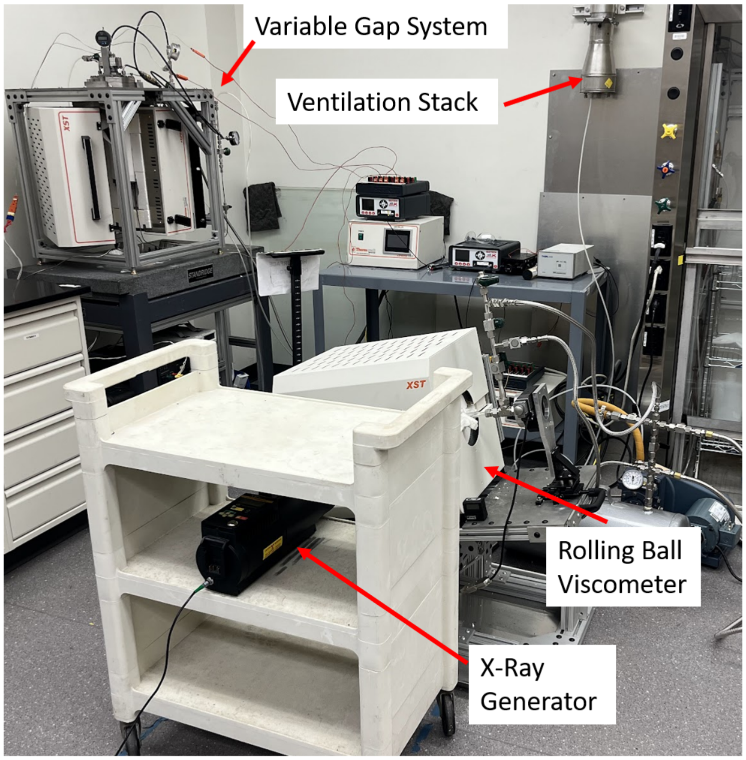

Figure 11. Both the rolling ball viscometer and variable gap system with the integrated ventilation stack.

5. CONCLUSION

In general, thermal conductivity and viscosity are not well characterized for many key molten salt systems of interest to MSR developers. To address this issue, a variable gap system for thermal conductivity, and a rolling ball viscometer were tested on the key chloride pseudo-binary system, NaCl-KCl, to generate property datasets that may be added to the literature. These tests were also conducted to demonstrate the feasibility of performing accurate measurements on uranium-bearing systems, which are particularly lacking in terms of thermophysical characterization. Thermal conductivity measurements with NaCl-KCl showed good agreement with kinetic theory and ab initio modeling, both in terms of magnitude and temperature dependence. Viscosity measurements with NaCl-KCl show reasonable agreement with independent experimental studies, and the impact of increasing NaCl concentration has been shown to increase the viscosity of the mixture. A dedicated, high-throughput x-ray system was arranged for the viscometer, and both systems were integrated with a ventilation system for off-gassing of radioactive material. Both systems are now prepared for measurements with uranium-bearing salts, with the target of conducting such measurements in FY24.

6. REFERENCES

[1] C. Agca and J. W. McMurray. Empirical estimation of densities in nacl-kcl-ucl3 and nacl-kcl-ycl3 molten salts using redlich-kister expansion. *Chemical Engineering Science*, 247:117086, 2022.

[2] X.-H. An, J.-H. Cheng, H.-Q. Yin, L.-D. Xie, and P. Zhang. Thermal conductivity of high temperature fluoride molten salt determined by laser flash technique. *International Journal of Heat and Mass Transfer*, 90:872–877, 2015.

[3] H. Andrews and S. Phongikaroon. Development of an experimental routine for electrochemical and laser-induced breakdown spectroscopy composition measurements of SmCl3 in LiCl-KCl eutectic salt systems. *Nuclear Technology*, 205(7):891–904, 2019.

[4] J. C. Ard, J. A. Yingling, K. E. Johnson, J. Schorne-Pinto, M. Aziziha, C. M. Dixon, M. S. Christian, J. W. McMurray, and T. M. Besmann. Development of the molten salt thermal properties database-thermochemical (mstdb- tc), example applications, and licl- rbcl and uf3- uf4 system assessments. *Journal of Nuclear Materials*, 563:153631, 2022.

[5] B. R. Betzler, F. Heidet, B. Feng, C. Rabiti, T. Sofu, and N. R. Brown. Modeling and simulation functional needs for molten salt reactor licensing. *Nuclear Engineering and Design*, 355:110308, 2019.

[6] A. Birri, R. Gallagher, C. Agca, J. McMurray, and N. D. B. Ezell. Application of the redlich-kister expansion for estimating the density of molten fluoride psuedo-ternary salt systems of nuclear industry interest. *Chemical Engineering Science*, 260:117954, 2022.

[7] A. Birri, N. Termini, P. Rose, S. Chapel, H. Andrews, and N. D. Bull Ezell. Development and demonstration of a rolling ball viscometer for molten salts with near-minimum liquidus naclkcl. *Thermal Science and Engineering Progress*, 44:102029, 2023.

[8] T. Birri, R. C. Gallagher, N. Russell, N. Termini, P. Rose Jr, and N. D. Ezell. Fy22 progress report on viscosity and thermal conductivity measurements of molten salts. Technical report, Oak Ridge National Lab.(ORNL), Oak Ridge, TN (United States), 2022.

[9] E. Blandford, K. Brumback, L. Fick, C. Gerardi, B. Haugh, E. Hillstrom, K. Johnson, P. F. Peterson, F. Rubio, F. S. Sarikurt, S. Sen, H. Zhao, and N. Zweibaum. Kairos power thermal hydraulics research and development. *Nuclear Engineering and Design*, 364:110636, 2020.

[10] M. Bu, T. Feng, and G. Lu. Prediction on local structure and properties of licl-kcl-alcl3 ternary molten salt with deep learning potential. *Journal of Molecular Liquids*, 375:120689, 2023.

[11] M. Bu, W. Liang, and G. Lu. Molecular dynamics simulations on alcl3-licl molten salt with deep learning potential. *Computational Materials Science*, 210:111494, 2022.

[12] M. Bu, W. Liang, G. Lu, and J. Yu. Local structure elucidation and properties prediction on kcl–cacl2 molten salt: a deep potential molecular dynamics study. *Solar Energy Materials and Solar Cells*, 232:111346, 2021.

[13] J. Cooke. Development of the variable-gap technique for measuring the thermal conductivity of fluoride salt mixtures. Technical report, OAK RIDGE NATIONAL LAB., TENN., 1973.

[14] K. Duemmler, Y. Lin, M. Woods, T. Karlsson, R. Gakhar, and B. Beeler. Evaluation of thermophysical properties of the licl-kcl system via ab initio and experimental methods. *Journal of Nuclear Materials*, 559:153414, 2022.

[15] K. Duemmler, M. Woods, T. Karlsson, R. Gakhar, and B. Beeler. An ab initio molecular dynamics investigation of the thermophysical properties of molten nacl-mgcl2. *Journal of Nuclear Materials*, 570:153916, 2022.

[16] N. Ezell, R. C. Gallagher, C. Agca, and J. McMurray. Thermal property characterization of molten salt reactor–relevant salts. Technical report, Oak Ridge National Lab.(ORNL), Oak Ridge, TN (United States), 2021.

[17] J. O. Flores, R. Konings, and A. Smith. Using the quasi-chemical formalism beyond the phase diagram: Density and viscosity models for molten salt fuel systems. *Journal of Nuclear Materials*, 561:153536, 2022.

[18] R. C. Gallagher, A. Birri, N. Russell, and N. D. B. Ezell. Design and performance of a variable gap system for thermal conductivity measurements of high temperature, corrosive, and reactive fluids. *International Journal of Heat and Mass Transfer*, 192:122763, 2022.

[19] R. C. Gallagher, A. Birri, N. G. Russell, A.-T. Phan, and A. E. Gheribi. Investigation of the thermal conductivity of molten lif-naf-kf with experiments, theory, and equilibrium molecular dynamics. *Journal of Molecular Liquids*, 361:119151, 2022.

[20] A. Gheribi, D. Corradini, L. Dewan, P. Chartrand, C. Simon, P. A. Madden, and M. Salanne. Prediction of the thermophysical properties of molten salt fast reactor fuel from first-principles. *Molecular Physics*, 112(9-10):1305–1312, 2014.

[21] A. E. Gheribi and P. Chartrand. Thermal conductivity of molten salt mixtures: Theoretical model supported by equilibrium molecular dynamics simulations. *The Journal of chemical physics*, 144(8), 2016.

[22] L. Jorgensen. 19 - thorcon reactor. In T. J. Dolan, editor, *Molten Salt Reactors and Thorium Energy*, pages 557–564. Woodhead Publishing, 2017.

[23] T. Y. Karlsson, S. C. Middlemas, M.-T. Nguyen, M. E. Woods, K. R. Tolman, V.-A. Glezakou, S. D. Herrmann, J. Schorne-Pinto, R. D. Johnson, S. E. Reddish, et al. Synthesis and thermophysical property determination of nacl-pucl3 salts. *Journal of Molecular Liquids*, page 122636, 2023.

[24] S. F. Katyshev. *Svoystva rasplavov smesey galogenidov shchelochnykh metallov, tsirkoniy, gafniy i uran*. PhD thesis, Ural State Technical University, 2001.

[25] C. S. Kim. Thermophysical properties of stainless steels. Technical report, Argonne National Lab., Ill.(USA), 1975.

[26] H. Kim, C. Kwon, S. Ham, J. Lee, S. J. Kim, and S. Kim. Physical properties of kcl-ucl3 molten salts as potential fuels for molten salt reactors. *Journal of Nuclear Materials*, 577:154329, 2023.

[27] D. Leblanc and C. Rodenburg. Integral molten salt reactor. In *Molten Salt Reactors and Thorium Energy*, pages 541–556. Elsevier, 2017.

[28] T. Lichtenstein, L. Gardner, and M. Rose. Property measurements of the nacl-pucl3 molten salt system. Technical report, Argonne National Lab.(ANL), Argonne, IL (United States), 2022.

[29] B. Lu, E. Williams, J. Mauck, M. Howard, R. Wood, and E. L. Quinn. Development and assessment of a diversity and defense-in-depth strategy for the terrapower twr-p advanced nuclear power plant. *Nuclear Technology*, 202(2-3):101–105, 2018.

[30] H. Luo, S. Xiao, S. Wang, P. Huai, H. Deng, and W. Hu. Molecular dynamics simulation of diffusion and viscosity of liquid lithium fluoride. *Computational Materials Science*, 111:203–208, 2016.

[31] X. Lv, C. Chen, Z. Han, C. Guan, and Z. Xu. Shear viscosities and thermal conductivity of naf-alf3 molten salts: A non-equilibrium molecular dynamics study. *Journal of Fluorine Chemistry*, 241:109675, 2021.

[32] X. Lv, Z. Han, J. Chen, L. Jiang, Z. Xu, and Q. Liu. First-principles molecular dynamics study of ionic structure and transport properties of lif-naf-alf3 molten salt. *Chemical Physics Letters*, 706:237–242, 2018.

[33] X. Lv, Z. Xu, J. Li, J. Chen, and Q. Liu. Theoretical investigation on local structure and transport properties of nafalf3 molten salts under electric field environment. *Journal of Molecular Structure*, 1117:105–112, 2016.

[34] J. W. Mcmurray, K. Johnson, C. Agca, B. R. Betzler, D. J. Kropaczek, T. M. Besmann, D. Andersson, and N. Ezell. Roadmap for thermal property measurements of molten salt reactor systems. Technical report, Oak Ridge National Lab.(ORNL), Oak Ridge, TN (United States), 2021.

[35] I. G. Murgulescu and S. Zuca. Viscosite des melanges binaires de sels fondus les systemes-KCl+ NaCl KCl+ KBr PbBr2+ KBr. *Revue Roumaine de Chimie*, 10:129, 1965.

[36] M.-T. Nguyen, V.-A. Glezakou, J. Lonergan, B. McNamara, P. D. Paviet, and R. Rousseau. Ab initio molecular dynamics assessment of thermodynamic and transport properties in (k, li) cl and (k, na) cl molten salt mixtures. *Journal of Molecular Liquids*, 326:115262, 2021.

[37] J. Oishi and T. Kimura. Thermal expansion of fused quartz. *Metrologia*, 5(2):50, apr 1969.

[38] C. Robelin and P. Chartrand. A viscosity model for the (naf+ alf3+ caf2+ al2o3) electrolyte. *The Journal of Chemical Thermodynamics*, 43(5):764–774, 2011.

[39] A. Rodriguez, S. Lam, and M. Hu. Thermodynamic and transport properties of lif and flibe molten salts with deep learning potentials. *ACS Applied Materials & Interfaces*, 13(46):55367–55379, 2021.

[40] Z. Rong, J. Ding, W. Wang, G. Pan, and S. Liu. Ab-initio molecular dynamics calculation on microstructures and thermophysical properties of nacl–cacl2–mgcl2 for concentrating solar power. *Solar Energy Materials and Solar Cells*, 216:110696, 2020.

[41] Z. Rong, G. Pan, J. Lu, S. Liu, J. Ding, W. Wang, and D.-J. Lee. Ab-initio molecular dynamics study on thermal property of nacl–cacl2 molten salt for high-temperature heat transfer and storage. *Renewable Energy*, 163:579–588, 2021.

[42] M. Rose, L. Gardner, T. Lichtenstein, S. Thomas, and E. Wu. Property measurements of nacl-ucl3 and nacl-kcl-ucl3 molten salts. Technical report, Argonne National Laboratory (ANL), Argonne, IL (United States), 2023.

[43] P. B. Rose Jr, N. D. B. Ezell, R. C. Gallagher, and A. J. Martin. Radiographic rolling ball viscometer. *Transactions of the American Nuclear Society*, 124(1):230–232, 2021.

[44] M. Smirnov, V. Khokhlov, and E. Filatov. Thermal conductivity of molten alkali halides and their mixtures. *Electrochimica acta*, 32(7):1019–1026, 1987.

[45] K. Sorensen. Liquid-fluoride thorium reactor development strategy. In J.-P. Revol, M. Bourquin, Y. Kadi, E. Lillestol, J.-C. de Mestral, and K. Samec, editors, *Thorium Energy for the World*, pages 117–121, Cham, 2016. Springer International Publishing.

[46] N. Termini, A. Birri, S. Henderson, and N. D. Bull Ezell. An overview of the molten salt thermal properties database–thermophysical, version 2.1.1 (mstdb-tp v.2.1.1). Technical report, Oak Ridge National Lab.(ORNL), Oak Ridge, TN (United States), 2023.

[47] R. Towell, N. Collaboration, et al. Development of a university molten salt research and test reactor. In *APS Division of Nuclear Physics Meeting Abstracts*, volume 2019, pages SK–007, 2019.

[48] E. Van Artsdalen and I. Yaffe. Electrical conductance and density of molten salt systems: Kcl–licl, kcl–nacl and kcl–ki. *The Journal of Physical Chemistry*, 59(2):118–127, 1955.

[49] H. Yin, J. Lin, B. Hu, W. Liu, X. Guo, Q. Liu, and Z. Tang. Thermodynamic description of the constitutive binaries of the nacl-kcl-ucl3-pucl3 system. *Calphad*, 70:101783, 2020.

[50] J. Yingling, J. Schorne-Pinto, M. Aziziha, J. Ard, A. Mofrad, M. Christian, C. Dixon, and T. Besmann. Thermodynamic measurements and assessments for licl-nacl-kcl-ucl3 systems. *The Journal of Chemical Thermodynamics*, 179:106974, 2023.

[51] G. Young and T.-L. Sham. Initial assessment of metallurgical interaction of clad/base metal systems. Technical report, Argonne National Lab.(ANL), Argonne, IL (United States), 2018.